Rubidium hydrazinidoborane: Synthesis, characterization and hydrogen release properties

Carlos Castilla-Martinez, Dominique Granier, Christophe Charmette, Guillaume Maurin, Pascal Yot, Umit Demirci

Rubidium hydrazinidoborane: synthesis, characterization and hydrogen release properties

Carlos A. Castilla-Martinez,[1] Dominique Granier,[2] Christophe Charmette,[1] Guillaume Maurin,[2] Pascal G. Yot,[2] Umit B. Demirci [1]*

[1] Institut Européen des Membranes, IEM – UMR 5635, Univ Montpellier, ENSCM, CNRS, Montpellier, France

[2] Institut Charles Gerhardt Montpellier, ICGM – UMR 5253, Univ Montpellier, ENSCM, CNRS, Montpellier, France

* umit.demirci@umontpellier.fr

Abstract

In this work we present rubidium hydrazinidoborane $RbN_2H_3BH_3$ (RbHB), the newest and last member of the alkali metal derivatives of hydrazine borane $N_2H_4BH_3$ (HB). It is shown that HB readily reacts with metallic rubidium in THF at room temperature to form RbHB under argon atmosphere. The molecular and crystal structures of this new compound are discussed on the basis of FTIR spectroscopy, ^{11}B MAS NMR spectroscopy, and powder X-ray diffraction analyses. RbHB crystallizes in a monoclinic $P2_1$ (No. 4) unit cell where each Rb^+ cation adopts octahedral coordination surrounded by six $[N_2H_3BH_3]^-$ anions, which are two more than for e.g. $LiN_2H_3BH_3$ (with tetrahedral coordination) in accordance with the larger size of Rb^+. RbHB is isostructural to potassium hydrazinidoborane $KN_2H_3BH_3$. Its dehydrogenation properties, evaluated by using thermogravimetric analysis, differential scanning calorimetry, and isothermal analysis, are compared to those of the parent HB as well as to analogous compounds in order to evaluate the potential of RbHB as hydrogen storage material. According to the presented data, the dehydrogenation properties of RbHB are much better than those of HB and are comparable to those of the lithium derivative. Our main results are reported therein.

Keywords

Hydrazine borane; Hydrazinidoborane; Hydrogen storage; Rubidium.

1. Introduction

Energy is one of the most critical issues for humanity, and it is expected that the energy demand will rise by up to 30% by 2040 [1]. The primary source of energy nowadays is based on fossil fuels, but their consumption in large scale has led to the release of pollutants and greenhouse gases directly into the atmosphere, causing phenomena such as global warming, with all the negative consequences that these imply [2]. Besides, fossil fuels are limited resources that are being depleted rapidly.

One of the alternatives to circumvent this issue is the use of hydrogen as an energy carrier because this fuel is clean and nontoxic. As an element, hydrogen is the most abundant in the universe and its molecular counterpart H_2 can be produced by a variety of methods [3-6]. One of the major challenges for the use of hydrogen as a fuel is its storage. Currently, various approaches are under investigation: hydrogen can be stored by compression in high-pressure gas cylinder, as a liquid in cryogenic tank, or stored in a host material. There are some requirements that a given technology must have to be possibly considered for hydrogen storage, such as high gravimetric/volumetric hydrogen storage capacity, reversibility of storage, stability in use, and cycle life [6-8]. On this basis, a series of materials (e.g. metal hydrides, carbonaceous porous hosts, metal organic frameworks, and inorganic compounds) have emerged owing to high hydrogen storage capacities [9-12].

Boron and nitrogen-based compounds have received particular attention as chemical hydrogen storage materials [13-16]. Ammonia borane NH_3BH_3 (AB) is a typical example. It is a crystalline solid at ambient conditions that was reported for the first time in 1955 [17], and since then it has been widely investigated for hydrogen storage [18,19]. This material shows high gravimetric hydrogen density with 19.6 wt % H, and is able to release, exothermically and thus irreversibly, 1 equiv H_2 between 80-105 °C, then an additional 1.2-1.4 equiv H_2 between 120-200 °C, and finally the residual amount of hydrogen above 500 °C. However; there are some problems with this process: reaction rates are slow; undesired by-products like borazine $B_3N_3H_6$, ammonia NH_3 and diborane B_2H_6 can be formed; and the solid polymeric residue is of complex composition [20]. In other words, AB in pristine state is not suitable for hydrogen storage.

Hydrazine borane $N_2H_4BH_3$ (HB) is another boron and nitrogen-based compound that has been studied as hydrogen storage material [21]. HB is a derivative of AB: i.e., one protic hydrogen $H^{\delta+}$ of AB is substituted by an NH_2 group [22]. HB possesses a gravimetric hydrogen density of 15.4 wt % H, and it has four protic hydrogens ($H^{\delta+}$) and just three hydridic hydrogens ($H^{\delta-}$). The dehydrogenation of HB starts at about 60 °C, and the borane loses 2 equiv H_2 up to 250 °C, together with hazardous and toxic by-products (like N_2H_4 and NH_3). Worse, a shock-sensitive residue forms when HB is heated above 300 °C [23,24]. Accordingly, derivatives of it obtained by chemical modification have been developed.

Alkali metal hydrazinidoboranes $MN_2H_3BH_3$ (MHB) are obtained by substitution of one of the protic $H^{\delta+}$ of the middle NH_2 of HB by an alkali cation M^+, which results in an equivalent number of $H^{\delta+}$ and $H^{\delta-}$ in the as-formed ionic compound. Usually, MHB is synthesized by reaction of HB with a metal hydride MH. The first hydrazinidoborane that has been synthesized is $LiN_2H_3BH_3$ (LiHB; 11.7 wt % H). Wu et al. [25] and Moury et al. [26] reported two different phases of LiHB by ball milling, in different conditions, an equimolar mixture of HB and LiH. The former group obtained the high-temperature phase α-LiHB (monoclinic, s.g. $P2_1/c$), while the latter group reported the low-temperature phase β-LiH (orthorhombic, s.g. *Pbca*). The phase transition takes place at around 90 °C and then α-LiHB dehydrogenates while liberating 2.6 equiv H_2 up to 150 °C. Another derivative is $NaN_2H_3BH_3$ (NaHB; 8.9 wt % H; monoclinic, s.g. $P2_1/n$). It has to be prepared at −30 °C [27], because of the high reactivity of NaH with HB at ambient conditions (−27.7 kJ mol^{-1}) [28]. NaHB starts to release H_2 below 60 °C, and is capable of liberating 2.6 equiv H_2 in the range 60-150 °C (together with traces of both N_2 and NH_3) [27]. A last derivative of HB is $KN_2H_3BH_3$ (KHB; 7.2 wt % H; monoclinic, s.g. $P2_1$). It has to be synthesized in stainless steel vessel and in THF for safety reasons [29], since the reaction between KH and HB is highly exothermic (70.3 kJ mol^{-1}) [28]. KHB shows slightly better dehydrogenation properties than NaHB and LiHB do, with a first dehydrogenation step peaking at 52 °C [29]. With the help of computational calculations, the role of the M^+ cation was predicted to be crucial as it is believed to drive the formation of the complex intermediate $M–H\cdots H_3N_2BH_2$ [30,31]. This is known as the "metal cation driven hydride-transfer" mechanism that was first reported for alkali amidoboranes MNH_2BH_3, namely the alkali derivatives of AB [32,33]. However the dehydrogenation mechanism is more complex, as with amidoboranes [34].

Studying the isotopomer $LiN_2H_3BD_3$, Tan et al. brought to light occurrence of counterintuitive homopolar $H^{\delta+}\cdots H^{\delta+}$ and $D^{\delta-}\cdots D^{\delta-}$ reactions resulting in the formation of H_2 and D_2 (together with heteropolar $H^{\delta+}\cdots H^{\delta-}$ reactions leading to HD) [35].

No other HB derivatives have been reported so far. There have been efforts to synthesize $Mg(N_2H_3BH_3)_2$ (11.6 wt % H) or $Ca(N_2H_3BH_3)_2$ (9.3 wt% H) by ball milling MgH_2 or CaH_2 with 2 equiv HB, but all attempts failed [28]. We are continuing to target these alkaline-earth derivatives while exploring alternative synthesis protocols. Chemical modification is an efficient strategy in getting derivatives of HB (as well as of AB) with improved dehydrogenation properties in terms of temperature, kinetics, and H_2 purity. We therefore regard as being crucial to obtain and study new derivatives. There are three reasons for this. First, it is important to increase our knowledge and fundamental understanding of boron and nitrogen-based materials through new compounds. Second, they may widen the prospects for hydrogen storage applications. Third, they might open up new opportunities. Accordingly, in this work, we present a new derivative, namely rubidium hydrazinidoborane $RbN_2H_3BH_3$ (RbHB; 4.65 wt %), which is isostructural (monoclinic, s.g. $P2_1$) to KHB.

2. Experimental

2.1. Materials

Hydrazine hemisulfate $N_2H_4{\cdot}½H_2SO_4$ (≥98%), sodium borohydride $NaBH_4$ (≥98%), and anhydrous 1,4-dioxane (≥99.8%) were purchased from Sigma-Aldrich and used for the synthesis of HB according to a procedure we reported elsewhere [24]. All the manipulations were done in an argon-filled glovebox (MBraun M200B; O_2 < 0.1 ppm and H_2O < 0.1 ppm) and a Schlenk line under argon atmosphere. Rubidium (ingot, 99.6%, Sigma-Aldrich) and extra dry THF (99.5%, Acros Organics) were used for synthesis of RbHB in the glovebox at ambient temperature. It is worth mentioning that we preferred Rb to RbH for three reasons. (*i*) RbH has not been found to be available commercially. (*ii*) Using RbH supposes a lab-preparation of it and a subsequent reaction with HB; this is a two-step process, whereas the approach proposed herein is a one-step

process. (*iii*) As reported elsewhere [36], the use of RbH is not convenient, for safety reasons, because of its high reactivity (leading to highly exothermic processes).

2.2. Synthesis

HB readily reacts with Rb, as AB does [36]. Accordingly, for evident safety reasons, our syntheses were integrally performed in the glovebox where the O_2 and H_2O concentrations are below 0.1 ppm; in our conditions, we are not able to fix/change the reaction temperature and the reactions were performed at ambient temperature. Typically (Figure S1), HB (246 mg, 5.36 mmol) was dissolved in 20 mL of THF and poured into one flask that contained Rb (400 mg, 4.68 mmol). Release of H_2 started immediately. The reaction was left under stirring for 30 h. After, the remaining rubidium was collected (90 mg, 1.05 mmol). The solid precipitate was washed two times with THF and two times with 1,4-dioxane, dried under vacuum and recovered. At best it was possible to recover 393 mg of product (corresponding to a yield of 83% with respect to the reacted alkali metal).

2.3. Methods

The as-obtained RbHB was analyzed by solid-state ^{11}B magic angle spinning nuclear magnetic resonance (MAS NMR; Varian VNMR400, 128.31 MHz) and Fourier Transformed Infrared (FTIR) spectroscopy (NEXUS instrument, ThermoFisher Scientific; equipped with an attenuated total reflection accessory from 600 to 4000 cm^{-1} wavelength). The dehydrogenated RbHB samples were analyzed in the same way.

The crystalline structure of RbHB was determined by powder X-ray diffraction (PXRD) analyses. A PANalytical X'Pert Multipurpose diffractometer equipped with an X'Celerator detector (Cu-Kα1/α2 radiation λ = 1.5418 Å, 45 kV, 30 mA) equipped with fixed divergence slits was used. The pattern was collected using Bragg-Brentano geometry on a spinning zero background sample holder loaded in the glovebox. The powder was protected using a Kapton foil stuck onto the sample holder with Apiezon grease (H quality) to prevent any O_2 and H_2O contamination. The diffraction pattern was recorded in the 15-80° angle range in 2θ using a step size of 0.017, and a scan step time of about 450 seconds. The crystalline state of the dehydrogenated solids was controlled using a Debye-Scherrer configuration (Cu-Kα1 radiation λ = 1.54059 Å). The samples

were filled in glass capillary of 0.5 mm diameter in the glovebox, sealed and then analyzed in the equipment.

The thermal behavior of RbHB was analyzed by thermogravimetric (TG) analysis (Netzsch STA 449 F1 Jupiter) that was coupled to a mass spectrometer (MS; Netzsch QMS 403 D Aëolos Quadro). It was also analyzed by simultaneous differential scanning calorimetry (DSC; Q600, TA Instruments).

The thermal behavior of RbHB was also analyzed at isothermal conditions (80, 100, 120 and 140 °C) in a stainless steel reactor. Inside the glovebox, 100 mg of sample was weighed, placed into the reactor and then closed tightly. Outside the glovebox, the reactor was connected to a pressure controller and immersed in an oil bath kept at the designated temperature. The dehydrogenation of the sample was followed by measuring the pressure change. The collected data were converted into mol H_2 per mol of RbHB (i.e. equiv H_2) and were plotted as a function of time.

2.4. Caution

Handling of HB-based materials must be done in the safest conditions. The solid residue of HB after heat treatment above 300°C produces a shock-sensitive material. Though such shock-sensitive solid has not been obtained with hydrazinidoboranes yet, care must be taken in any case; there is always a risk to form an instable by-product.

Otherwise, RbHB as well as the solids recovered after heat treatment at any temperature have to be “neutralized” by reaction (alcoholysis) with a small amount of heavy alcohol (e.g. isopropanol) under hood (release of some H_2). The as-formed borates are trashed in the container of alkaline aqueous wastes. (*ii*) Handling of Rb must be done under inert atmosphere, due to its high reactivity and the violent reaction (flash fire) that occurs when in contact with water/moisture.

A fast, quite “explosive”, reaction takes place between Rb and HB if they are put directly into contact in solid state. It is important to mention here that, at the beginning of this work, we tried to synthesize RbHB at 0°C, outside of the glovebox, using Schlenk glassware connected to a

vacuum-argon line. However, we faced some security issues (likely because of traces of moisture and/or oxygen) and we decided to continue our experiments directly in our glovebox (where the O_2 and H_2O concentrations are below 0.1 ppm). In doing so, we found the safest conditions to prepare RbHB.

3. Results and discussion

3.1. Preliminary comments

Our first attempt to synthesize RbHB (under argon atmosphere) was to put Rb and HB in a round-bottom flask and then add extra-dry THF. We observed a violent reaction between both reactants. After different attempts, we found that it is of extreme importance to dissolve HB in THF before putting it onto Rb. In doing so (Figure S1), RbHB was synthesized in safer conditions a number of times. The same protocol could be used to target other derivative. For example, the cesium derivative should be readily obtained by reaction of Cs with HB in the same conditions (i.e. O_2 and H_2O-free atmosphere and extra-dry solvent).

RbHB is a white powder. We looked for suitable (anhydrous) organic solvents. It is insoluble in THF, dioxane, and toluene. We also checked its behavior in the presence of a protic solvent. RbHB reacts with water and ethanol (by solvolysis) and the reaction is accompanied by H_2 generation. These observations are consistent with those made for the other alkali hydrazinidoboranes [25-27] and amidoboranes [15,37].

3.2. Molecular structure

The sample was analyzed by solid state ^{11}B MAS NMR spectroscopy and the spectrum compared to that of HB (Figure 1). The spectrum of HB shows a single signal (centered at –24 ppm) which split shape is due to quadrupolar coupling [38]. The spectrum of RbHB shows a comparable split signal at lower chemical shift (centered at –17.5 ppm), which is consistent with the substitution of one $H^{\delta+}$ by Rb^+. This indicates a different electronic arrangement in the N*B*H$_3$ environment of RbHB where –NH(Rb)– is a stronger donor complex with BH_3 [39]. This might also suggest shortening of the B–N bond of the anion $N_2H_3BH_3^-$ [15]. Interestingly, the N*B*H$_3$ signal of RbHB

is asymmetric and suggests prevalence of anisotropy around the boron atom [38]. In contrast, with the other hydrazinidoborane and amidoborane compounds [15,25-27], the signal has a symmetric resonance due to isotropy around the boron atom. We may thus suppose that the molecular degree of freedom is much less pronounced for RbHB.

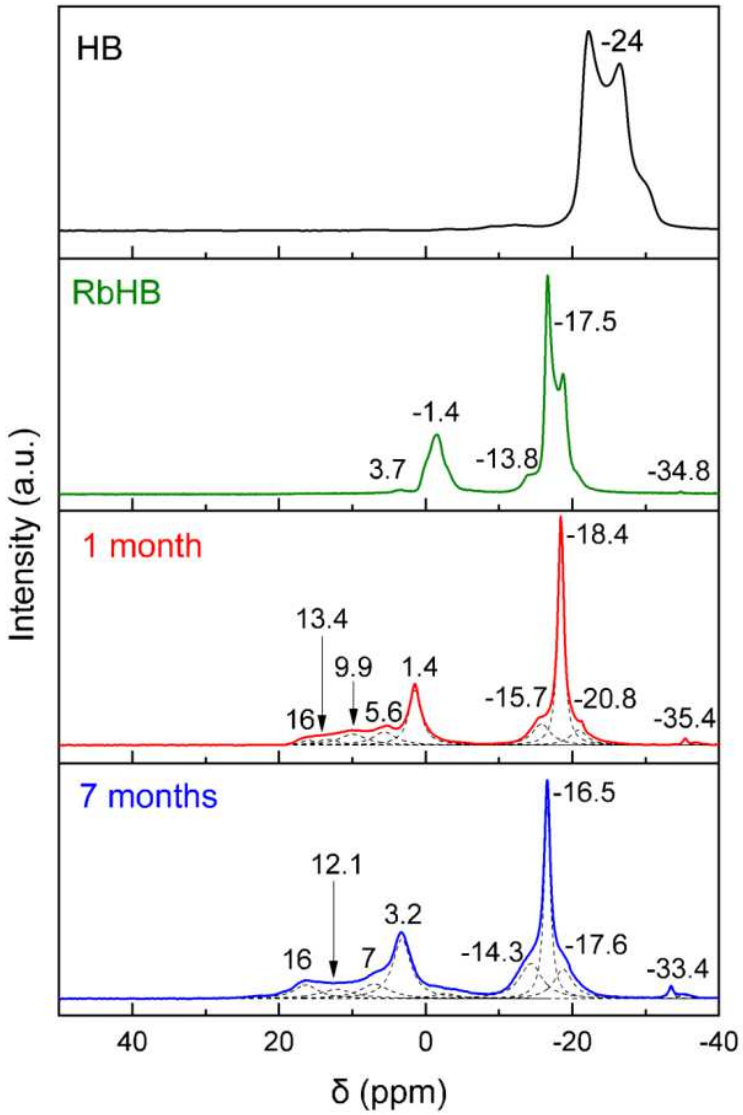

Figure 1. ^{11}B MAS NMR spectra of HB, RbHB, RbHB after 1 month (stored at room temperature and under argon atmosphere), and RbHB after 7 months. The signals for the samples stored 1 and 7 months were deconvoluted. The chemical shifts (in ppm) are indicated.

The ^{11}B MAS NMR spectrum of RbHB is also featured by four other signals of different intensities at −34.8, −13.8, −1.4 and +3.7 ppm. The first two signals are ascribed to BH$_4$ and N$_2B$H$_2$ environments respectively [40]. They may be due to some dehydrocoupling intermediates like the previously proposed ionic dimer of formulae [(MN$_2$H$_3$)$_2$BH$_2$]$^+$[BH$_4$]$^-$ [26,27]. The N$_2B$H$_2$ environment could also be interpreted as the occurrence of the complex Rb–H···H$_3$N$_2$BH$_2$ [30,31] or the dimer N$_2$H$_3$(Rb)BH$_2$N$_2$H$_2$(Rb)BH$_3$ [29]. The signal at −1.4 ppm is attributed to an N$_3B$H environment and that at +3.7 ppm to an BN$_4$ environment [41]. The presence of such environments implies the formation of highly dehydrogenated polymeric residue of RbHB. Dehydrocoupling is likely to happen because of a slow evolution of RbHB at room temperature, which besides could be aggravated during analysis (rotor rotation). Furthermore, we cannot rule out the hypothesis that such species may form during synthesis itself.

RbHB was analyzed by FTIR spectroscopy and the spectrum was compared to that of HB (Figure 2). The N–H stretching region is much different. For RbHB, there are fewer bands of lower intensity. Less intense bands are also observed at the N–H bending region. This observation indicates differences between N$_2$H$_4$– of HB and N$_2$H$_3$(Rb)– of RbHB in terms of electronic structure and binding strength. This is typical of a derivative where there are weaker interactions of H$^{\delta+}$ and H$^{\delta-}$ between molecules (because of longer distance due to the big Rb$^+$ cation) [42,43]. Regarding the B–H stretching region, RbHB presents bands at lower wavenumbers than HB does, also suggesting a different chemical environment for the B–H bonds and the BH$_3$ groups. The N–N stretching band shows a slight change; it is less intense for RbHB. In the B–N region, the signal peaking at 906 cm^{-1} for HB has red-shifted to 838 cm^{-1} for RbHB, indicating a stronger B–N bond, which is in good agreement with the downfield shift of the boron resonance (Figure 1). Shorter B–N bonds are typical of hydrazinidoboranes [25-29] and amidoboranes [15,36,39]. It is also to mention that the spectrum of RbHB is rather comparable to that of LiHB and NaHB (Figure S2). All of these spectroscopic observations are consistent with the formation of RbHB.

3.3. Stability

The stability of RbHB in solid state was investigated by ^{11}B MAS NMR and FTIR spectroscopy. Two RbHB samples were stored in the argon-filled glovebox for one and seven months after synthesis.

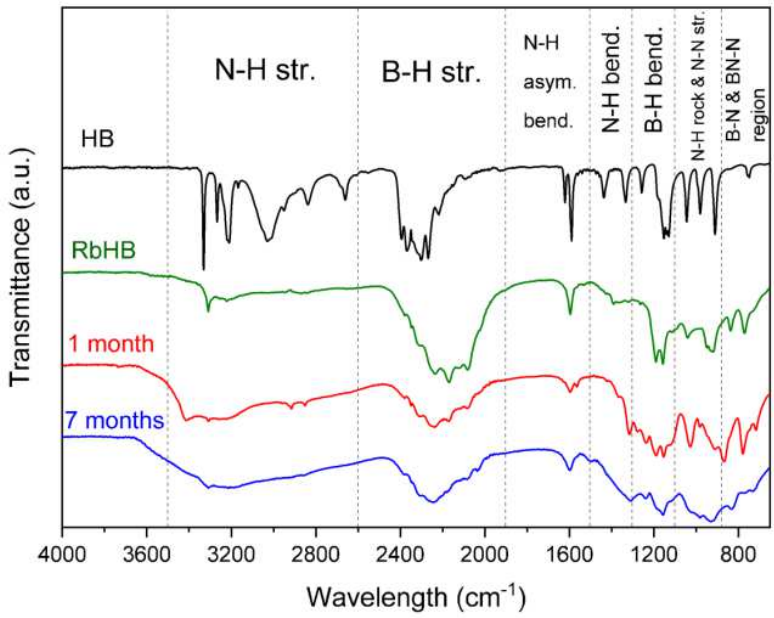

Figure 2. FTIR spectra of HB, RbHB, RbHB after 1 month (stored at room temperature and under argon atmosphere), and RbHB after 7 months. The bands have been assigned.

The ^{11}B MAS NMR spectra (Figure 1) show several changes. The most prominent one is the change of the signal at −17.5 ± 1 ppm, attributed to a N*B*H$_3$ environment which loses its initial asymmetric shape. It is symmetric, suggesting much higher isotropy around the boron atom [38]. The intensity of the signal at around −35 ppm and that of the hump at around −15 ppm are higher. The former signal is characteristic of a *B*H$_4$ environment. The latter one may be ascribed to an N$_2$*B*H$_2$ environment [40] . A broad signal of low intensity can be seen between 0 and −12 ppm and it can be attributed to N$_2$*B*H and N$_3$*B*H environments. Another broad signal deconvoluted into 4-5 signals appeared at positive chemical shifts. The signals at <+10 ppm are typical of tetravalent *B*N$_4$ environments; the other ones are due trivalent boron environments generally observed for borazine-linked polymeric species [39,41,44-48].

The FTIR analysis (Figure 2) revealed that the N–H stretching bands broaden with time. The broadening extends beyond 3400 cm^{-1}, which indicates the presence of polymeric compounds. Consistently, the B–H stretching bands become weaker in intensity.

In other words, RbHB is not stable at room temperature. It evolves by dehydrocoupling. Dimeric species as those discussed above form. With time, highly dehydrogenated polymeric species (e.g. polyiminoborane- and polyborazylene-like) form. It is worth mentioning that the AB derivative, $RbNH_2BH_3$, also undergoes slow decomposition at room temperature [36]. The reason is the size of the Rb^+ cation that can destabilize the molecule [49].

3.4. Crystal structure

The PXRD pattern of RbHB was first compared to that of HB (Figure 3). It does not exhibit any diffraction peaks of HB and can be considered as a pure phase. The broad peaks were identified from Kapton foil used to protect the solid. However, as suggested by the ^{11}B MAS NMR results, the presence of some amorphous dehydrogenated products cannot be discarded.

The PXRD pattern of RbHB was indexed as a single phase (cf. supplementary material (SM), Tables S1 and S2, and Figures S3 and 4): monoclinic $P2_1$ (No. 4) unit cell; $Z = 2$; $a = 5.8128(2)$ Å, $b = 6.7010(2)$ Å, $c = 5.8143(2)$ Å and $\beta = 108.915(2)°$. RbHB is isostructural to KHB [29], whereas α-LiHB and NaHB crystallize in different monoclinic cells ($P2_1/c$ and $P2_1/n$ respectively) [25,27]. As a derivative of AB, $RbNH_2BH_3$ shows a different monoclinic cell ($P2_1/c$) and a volume per formula unit of 94.24 $Å^3$ [36] which is slightly smaller than the volume per formula unit of 107.22 $Å^3$ of RbHB; this is consistent with the bigger size of the anion $N_2H_3BH_3^-$. The volume per formula unit of HB is also smaller with 80.154 $Å^3$ [25], which is consistent with the presence of the bulkier cation Rb^+ in RbHB.

In RbHB, the cation Rb^+ is octahedrally coordinated with 6 $[N_2H_3BH_3]^-$ anions (Figure S4). In $RbNH_2BH_3$ also, it was found a pseudo-octahedron around each Rb^+ cation [36]. The coordination number for Li^+, Na^+, and K^+ in the corresponding hydrazinidoboranes were lower, being 4, 5 and 4, respectively [26-29]. A higher coordination number is consistent with the bigger

size of Rb^+, i.e. a bigger surface for coordination with the anions $[N_2H_3BH_3]^-$ that may interact with Rb^+ through their two N and six H atoms.

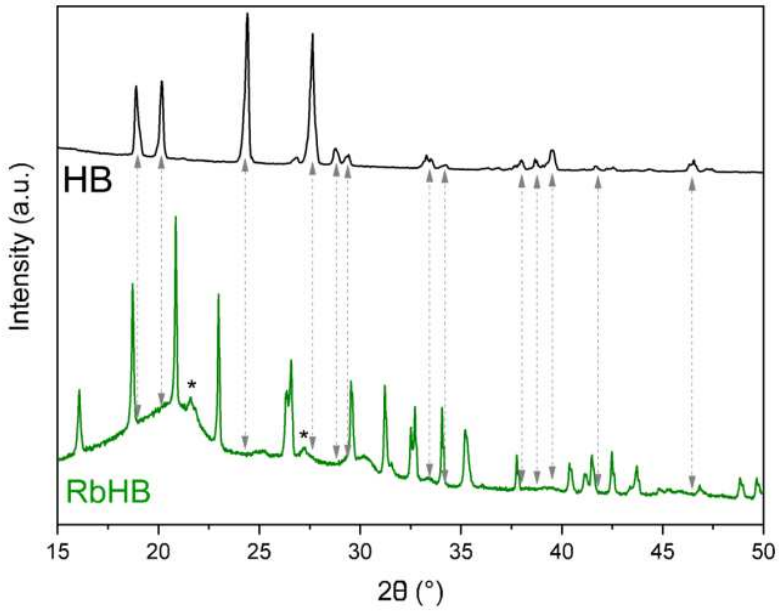

Figure 3. Comparison of the X-ray powder diffraction patterns of pure HB and RbHB. The stars indicate the peaks due to the Kapton foil used to prevent the samples from air and moisture.

For RbHB, the locations of the H atoms linked to the N and B atoms were computationally determined (cf. SM, and Figure S5), allowing to bring out interatomic distances. The shortest Rb···Rb distance was found to be 4.246 Å. This is slightly higher than the distance 4.025 Å calculated for $RbNH_2BH_3$ [36], which is explained by the bigger size of the anion $[N_2H_3BH_3]^-$. The shortest Rb···N distance was determined as 3.132 Å (vs 3.06 Å for $RbNH_2BH_3$). It is longer than the shortest distance in KHB (2.959 Å) [29], because of the bigger size of Rb^+ vs K^+. The Rb···H–B and Rb···H–N distances resulting from the geometry optimization are between 2.56 and 3.10 Å. The N–N distance is 1.43 Å as obtained from the Rietveld refinement, and it is similar to that observed for HB (1.41 Å) [24] and slightly shorter compared to the bond determined in the case of the other MHBs (α-LiHB 1.469 Å; β-LiHB 1.495 Å; NaHB 1.46 Å; KHB 1.47 Å) [25-

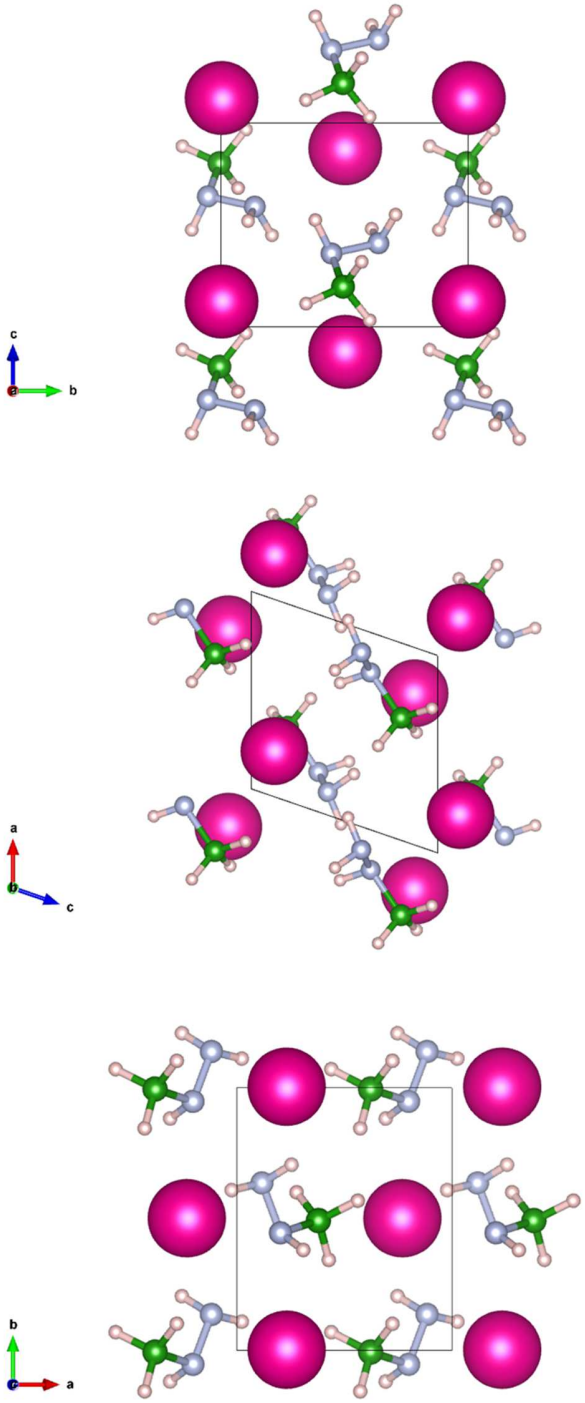

Figure 4. Crystal structure of $RbN_2H_3BH_3$ along the [100], [010], and [001] directions. H, B, and N atoms are represented by pink, green, and blue spheres. Rb atoms are represented by fuchsia spheres.

27,29]. The B–N bond was determined as being of 1.55 Å, which is consistent with the values 1.54-1.55 Å found for LiHB, NaHB and KHB [26-29]. The bond is besides shorter than the B–N bond of HB (1.59 Å) [24,25]. This is in good agreement with the aforementioned shortening of the B–N bond by Rb^+ insertion as suggested by ^{11}B MAS NMR and FTIR spectroscopy. All of the data are in favor of the formation of an ionic salt where the anion $[N_2H_3BH_3]^-$ underwent strong electronic rearrangement due to the presence of Rb^+.

In RbHB, the average intermolecular $H^{\delta+}\cdots H^{\delta-}$ distances were found to be about 2.84 Å. This is slightly longer than the corresponding data reported in the parent HB (2.246 Å) [24], and in the other alkali derivatives: α-LiHB (2.01 Å) [25], β-LiHB (2.25 Å) [26], NaHB (2.41 Å) [27], and KHB (2.357 Å) [29].

3.5. Thermal analysis

Thermolytic decomposition of RbHB was studied by TG analysis (heating rate of 5 °C min^{-1}) and the generated gas was analyzed by MS. The material is stable up to ca. 60°C (Figure 5). Then, it starts to decompose. Over the range 60-100 °C, RbHB loses ca. 5 wt % of its initial weight, due to the release of H_2 and NH_3. Based on calculations made for LiHB, the formation of NH_3 can be explained by H-shift across the N–N bond (leading to $BH_3MN\cdots NH_3$) followed by breaking of the N···N link, the reaction being exothermic in nature [30]. This may explain the NH_3 release from RbHB in our conditions, and the bigger size of Rb^+ (allowing higher coordination with the N–N–B backbone) would be favorable to the aforementioned H-shift. The second decomposition step of our TG analysis takes place in the range 115-145 °C where the mass loss is low with 0.5 wt %. There is a third decomposition step between 150-200 °C, with a mass loss of 1.3 wt %. For both of these last two steps, only H_2 was detected by MS. The overall weight loss from 60 to 200 °C is thus 6.8 wt %. This is higher than the 4.65 wt% H carried by RbHB and such a difference may be explained by the loss of a significant amount of NH_3. In our conditions, there was no detection of any other volatile by-products (e.g. B_2H_6, N_2H_4, or $B_3N_3H_6$).

In terms of onset temperature of dehydrogenation, RbHB shows better dehydrogenation properties in comparison to HB, and is more or less comparable to LiHB. In contrast, NaHB and

KHB have better features. In terms of purity of the released H_2, LiHB, NaHB and KHB are more attractive [24-27]. One may however notice that the amount of the unwanted volatile products NH_3 seems to increase with the size of the alkali cation M^+ down in the group.

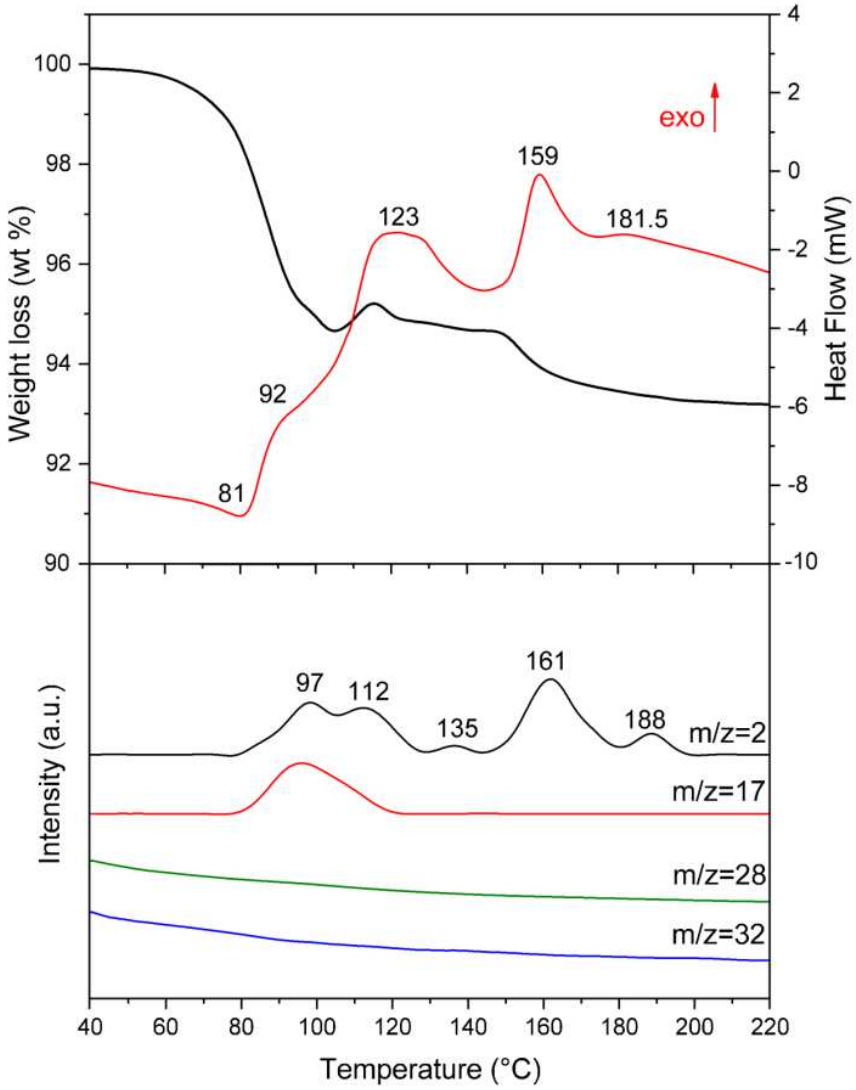

Figure 5. TGA-DSC (5°C min^{-1}) and MS results (*m/z* = 2, 17, 28, 32 for H_2, NH_3, B_2H_6 or N_2, N_2H_4 respectively) of RbHB. The peak temperatures (°C) observed by DSC and MS are given.

RbHB was also analyzed by DSC (Figure 5). The DSC profile clearly suggests a complex decomposition path. A first event, which is endothermic, peaks at 80 °C. As for HB, NaHB, and KHB [24,27,29], melting takes place and precedes the dehydrogenation of RbHB (Figure S6). Then follow several exothermic events. The DSC and MS analyses suggest five successive steps.

According to MS, these dehydrogenation steps peak at 97, 112, 135, 161, and 188 °C. The first dehydrogenation step is concomitant with a deammoniation step peaking at 95 °C. These results suggest a complex dehydrogenation mechanism. Due to the exothermicity of the dehydrogenation process (cf. SM, and Figures S7 and S8), rehydrogenation of the dehydrogenated samples is considered not possible under normal conditions [13-16], and if regeneration is considered, it should be done by other means [50].

Looking back to the TG analysis, we can see a slight gain of mass (hump) at around 110 °C. A similar feature was reported for HB, NaHB and KHB. This is explained by a "buoyancy effect" that takes place when the melted borane solidifies while releasing H_2 [24,29]. Foaming accompanies this effect which generally intensifies the aforementioned hump (Figure S6).

3.6. Dehydrogenation experiments

Experiments under isothermal heating were carried out in a stainless steel reactor at 80, 100, 120 and 140 °C. The dehydrogenation of RbHB is a two-step process (Figure 6). Similar profiles were reported for LiHB and NaHB for example [26,27], even though for RbHB the break in the slope is more prominent. The first step takes place in the first 23, 20, 17 and 13 minutes for the sample heated at 80, 100, 120 and 140 °C, respectively. Then the second step follows. The initial H_2 release rates, i.e. those determined for the first step, have been used to determine the apparent activation energy (cf. SM, and Figure S9). To do that it was assumed that RbHB releases H_2 only (the evolution of NH_3 as by-product was neglected for the calculation). An apparent activation energy of 30.1 kJ mol^{-1} was calculated. This value is lower compared to other boron and nitrogen-based materials. Pure ammonia borane and LiH-doped ammonia borane have respective apparent activation energies of 183 and 75 kJ mol^{-1}, calculated by the same method [51]. Another example is lithium amidoborane and $LiBH_4$-doped lithium amidoborane, whose apparent activation energies are of 71 and 61 kJ mol^{-1}, respectively [52]. In the case of hydrazinidoboranes, the calculated apparent activation energy for LiHB is 58 kJ mol^{-1} [26]; however, NaH-doped NaHB possesses lower activation energy of 14.4 kJ mol^{-1} [53]. This lower value for NaHB can be related to its better dehydrogenation properties.

The dehydrogenation curves (Figure 6) were further exploited to compare RbHB to HB [24], LiHB [26], and NaHB [27], all having been studied in identical experimental conditions. Heated at 100 °C, RbHB, HB and LiHB have comparable H_2 release results: they all release 0.60(5) equiv H_2 in 1 h. This is less than the 2.6 equiv H_2 liberated by NaHB. Heated at 140 °C for 1 h, RbHB releases 2 equiv H_2 vs 1.1 for HB. Slightly better performance was reported for LiHB with 2.2 equiv H_2. To sum up, RbHB has improved dehydrogenation properties in comparison to those of pristine HB, is comparable to LiHB, and is less attractive than NaHB. The destabilization effect of Rb^+ is confirmed. At this point, it would appear that there is no relation between the cation size and the thermal stability of the MHB compounds.

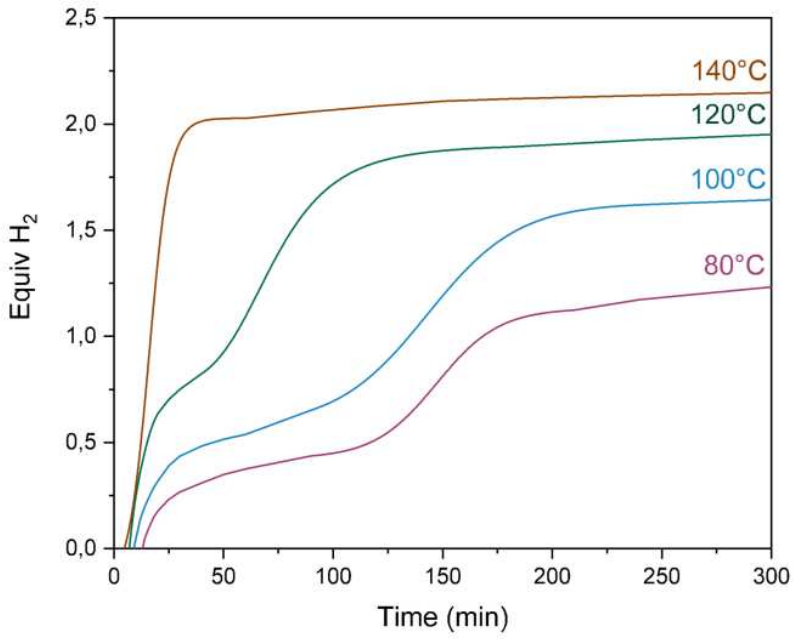

Figure 6. Time evolution of H_2 release from RbHB under heating at a constant temperature (80, 100, 120, and 140 °C).

3.7. Dehydrogenated samples

The solid residues recovered upon the completion of the isothermal experiments were analyzed by FTIR (Figure 7). The intensity of the N–H and B–H stretching bands decays as the heating temperature increases. A similar behavior can be observed for the signal assigned to the N–H

asymmetric bending. All of these bands almost disappeared for the solid heated at 140°C. This is consistent with the formation and release of H_2 from RbHB.

The solid residues were also analyzed by PXRD (Figure S10). There is no diffraction peak. The solids are amorphous, suggesting polymeric materials.

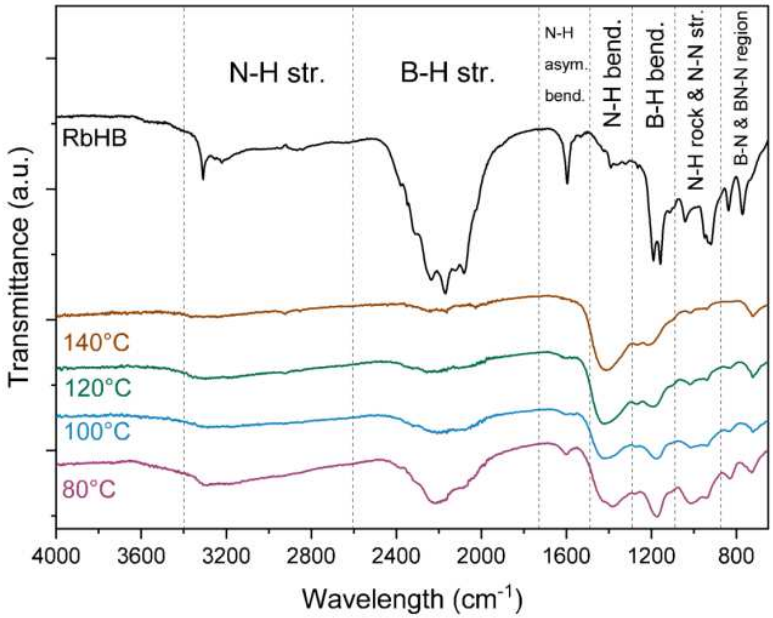

Figure 7. FTIR spectra of RbHB, and of the solid residues recovered upon heating a sample of RbHB at 80, 100, 120, or 140 °C for 24 h. The bands have been assigned.

Better identification was done by analyzing the solid residues by ^{11}B MAS-NMR (Figure 8). A resonance centered at −34.4 ppm appeared in all heated samples. This signal is characteristic of the BH_4 environment. As discussed above for the fresh RbHB, this boron environment may be explained by the formation of an ionic dimer like $[(RbN_2H_3)_2BH_2]^+[BH_4]^-$ [26,27]. The existence of such dimer implies an additional resonance due to a N_2BH_2 environment, and it can be seen at −16 ppm. The intensity of this signal decreases as the temperature of the isothermal experiment increases. Note that for the sample heated at 80 °C the asymmetric signal can be deconvoluted into two Gaussian signals centered at −14 and −17 ppm. The former is due to the N_2BH_2

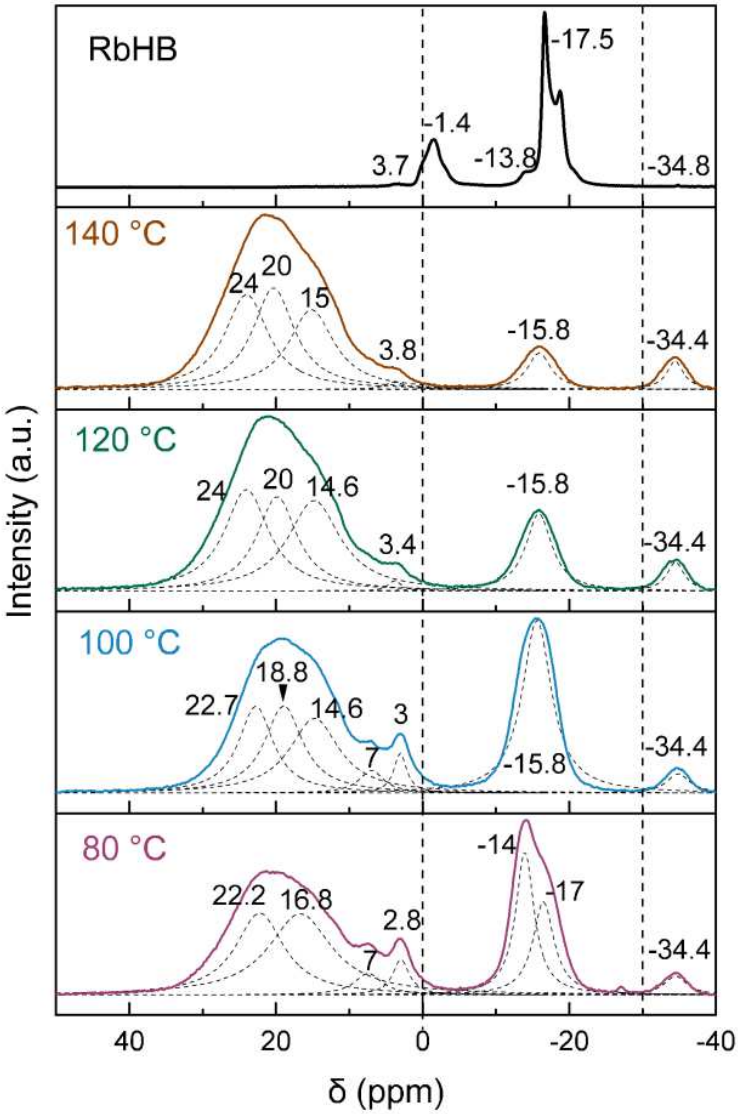

Figure 8. ^{11}B NMR spectra of RbHB, and of the solid residues recovered upon heating a sample of RbHB at 80, 100, 120, or 140 °C for 24 h. The signals for the solid residues were deconvoluted. The chemical shifts (in ppm) are indicated.

environment. The latter can be attributed to the N*B*H$_3$ environment, suggesting remaining RbHB and/or unreacted NH$_3$ groups. Referring to the literature dedicated to alkali derivatives of AB [32,33,42,49,54,55], several possible complex intermediates were tentatively identified via experimental analyses and theoretical calculations, and such intermediates (adapted to $N_2H_3BH_3^-$) might help in ascribing the aforementioned signals: for instance,

$[N_2H_4Rb]^+[BH_3(N_2H_2Rb)BH_3]^-$, Rb–H···$H_3N_2BH_2$, Rb–H···$RbN_2H_3BH_2N_2H_3BH_3$, $[RbN_2H_3BH_2RbN_2H_3]^+[BH_4]^-$.

The ^{11}B MS NMR spectra also show a broad signal at positive chemical shifts and which contribution is larger as the temperature of the isothermal experiment increases. They are typical of trivalent boron environments [44-48]. At lower temperatures (80 and 100 °C), there are also two signals centered around +2.8 and +7 ppm that could indicate the presence of a tetravalent BN_4 [41]. The broad signal between +10 and +40 ppm is composed of mainly three signals centered at +14, +20, and +24 ppm. They are due to the presence of borazine-linked polymeric species. The broadening of the signals is due to the quadrupolar effect of the trivalent boron, usually assigned to BN_2H and BN_3. It seems that like in the case of AB, dehydrocoupling of RbHB results in the formation of polyborazylene-like compounds. Further investigations may appear necessary to go further in the identification of the dehydrogenated residues, but as for AB and its derivatives, this is a task that has proven to be difficult [50]. This remains a challenge in our field.

4. Conclusions

We have synthesized rubidium hydrazinidoborane $RbN_2H_3BH_3$ (RbHB; 4.65 wt % H) for the first time. Spectroscopic and structural investigations on RbHB were carried out. The substitution of one $H^{\delta+}$ of $N_2H_4BH_3$ by Rb^+ has been successful as evidenced by ^{11}B MAS NMR and FTIR spectroscopy. The presence of Rb^+ has a destabilization effect on the anion $N_2H_3BH_3^-$. The destabilization is so important that the solid slightly evolves with time towards dehydrogenated polymeric compounds. The crystal structure of RbHB is monoclinic, with a space group $P2_1$ (No. 4); it is isostructural to KHB [29]. The cell parameters are such as a = 5.8128(2) Å, b = 6.7010(2) Å, c = 5.8143(2) Å, and β = 108.915°. Investigations on thermal properties of RbHB were also carried out, under heating at a constant rate (5 °C min^{-1}) and in isothermal conditions. RbHB has improved dehydrogenation properties in comparison to the parent HB. The destabilization effect of Rb^+ has been confirmed. The performance of RbHB is comparable to that of $LiN_2H_3BH_3$, but is less attractive than $NaN_2H_3BH_3$, in terms of onset temperature of dehydrogenation and H_2 release kinetics. Upon the evolution of H_2, an amorphous polymeric solid, mainly

polyborazylene-like, forms. Further investigation would be helpful in going further in the identification of this dehydrogenated solid, the reaction mechanisms, and the exact role that Rb^+ plays.

Synthesizing and analyzing a new compound like RbHB have provided a number of results that firstly add knowledge about boron and nitrogen-based materials. Secondly, the presented results have shown that the dehydrogenation properties of RbHB are interesting, but for an application in the field of chemical hydrogen storage, RbHB is not the best candidate. It is comparable to LiHB in terms of dehydrogenation properties whereas it carries less hydrogen (theoretical amount of 4.65 wt% H vs 11.7 wt % H). Thirdly, we now have one more HB derivative and future works could be to explore its potential as precursor of boron nitride-based ceramics; the presence of the alkali cation, as possible crystallization promoter [56], might allow getting highly crystalline boron nitride at low temperature or a crystalline structure different from the hexagonal one.

Acknowledgements

The authors acknowledge the Mexican National Council for Science and Technology CONACyT for the scholarship to CACM.

References

[1] International Energy Outlook 2016 – With Projections to 2040; The U.S. Energy Information Administration (EIA), Office of Energy Analysis, U.S. Department of Energy; Washington, DC, 2016. https://www.eia.gov/outlooks/ ieo/pdf/0484(2016).pdf.

[2] a) Parry I. Fossil-fuel subsidies assessed. Nature 2018;554:175–176; b) Wigley TML. The Paris warming targets: emissions requirements and sea level consequences. Clim Change 2018;147:31–45.

[3] Mazloomi K, Gomes C. Hydrogen as an energy carrier: prospects and challenges. Renew Sustain Energy Rev. 2012;16:3024–33.

[4] Zhang F, Zhao P, Niu M, Maddy J. The survey of key technologies in hydrogen energy storage. Int J Hydrogen Energy 2016;41:14535–52.

[5] Møller KT, Jensen TR, Akiba E, Li HW. Hydrogen – A sustainable energy carrier. Progr Nat Sci Mater Int 2017;1:34–40.

[6] Abdalla AM, Hossain S, Nisfindy OB, Azad AT, Dawood M, Azad AK. Hydrogen production, storage, transportation and key challenges with applications: a review. Energy Conv Manag 2018;165:602–7.

[7] Sinigaglia T, Lewiski F, Martins MES, Siluk JCM. Production, storage, fuel stations of hydrogen and its utilization in automotive applications – a review. Int J Hydrogen Energy 2017;42:24597–611.

[8] Durbin DJ, Malardier-Jugroot C. Review of hydrogen storage techniques for on board vehicle applications. Int J Hydrogen Energy 2013;38:14595–617.

[9] Lai Q, Paskevicius M, Sheppard DA, Buckley CE, Thornton AW, Hill MR, Gu Q, et al. Hydrogen storage materials for mobile and stationary applications: current state of the art. Chem Sus Chem 2015;8:2789–825.

[10] He T, Pachfule P, Wu H, Xu Q, Chen P. Hydrogen carriers. Nat Rev Mater 2016;1:16059.

[11] Ren J, Musyoka NM, Langmi HW, Mathe M, Liao S. Current research trends and perspectives on materials-based hydrogen storage solutions: a critical review. Int J Hydrogen Energy 2017;42:289–311.

[12] Berenguer-Murcia Á, Marco-Lozar JP, Cazorla-Amorós D. Hydrogen storage in porous materials: status, milestones, and challenges. Chem Rec 2018;18:900–12.

[13] Hamilton CW, Baker RT, Staubitz A, Manners I. B–N compounds for chemical hydrogen storage. Chem. Soc. Rev. 2009;38:279–93.

[14] Staubitz A, Robertson APM, Manners I. Ammonia borane and related as dihydrogen sources. Chem Rev 2010;110:4079–114.

[15] Chua YS, Chen P, Wu G, Xiong Z. Development of amidoboranes for hydrogen storage. Chem Commun 2011;47:5116–29.

[16] Moussa G, Moury R, Demirci UB, Şener T, Miele P. Boron-based hydrides for chemical hydrogen storage. Int J Energy Res 2013;37:825–42.

[17] Shore SG, Parry RW. The crystalline compound ammonia-borane, H_3NBH_3. J Am Chem Soc 1955;77:6084–5.

[18] Li H, Yang Q, Chen X, Shore SG. Ammonia borane, past as prolog. J Organomet Chem 2014;751:60–6.

[19] Akbayrak S, Özkar S. Ammonia borane as hydrogen storage materials. Int J Hydrogen Energy 2018;43:18592–606.

[20] Demirci UB. Ammonia borane, a material with exceptional properties for chemical hydrogen storage. Int J Hydrogen Energy 2017;42:9978–10013.

[21] Hügle T, Kühnel MF, Lentz D. Hydrazine borane: a promising hydrogen storage material. J Am Chem Soc 2009;131:7444–6.

[22] Yot PG, Yadav V, Ould-Amara S, Itiè JP, Demirci UB, Maurin G. Unraveling the mechanical behaviour of hydrazine borane (NH_2-NH_2-BH_3). Phys Chem Chem Phys 2018;20:2845–50.

[23] Goubeau VJ, Ricker E. Borinhydrazin und seine pyrolyseprodukte. Z Anorg Allg Chem 1961;*310*:123–42.

[24] Moury R, Moussa G, Demirci UB, Hannauer J, Bernard S, Petit E, van der Lee A, Miele P. Hydrazine borane: synthesis, characterization, and application prospects in chemical hydrogen storage. Phys Chem Chem Phy. 2012;14:1768–77.

[25] Wu H, Zhou W, Pinkerton FE, Udovic TJ, Yildirim T, Rush JJ. Metal hydrazinoborane $LiN_2H_3BH_3$ and $LiN_2H_3BH_3{\cdot}2N_2H_4BH_3$: crystal structures and high-extent dehydrogenation. Energy Environ Sci 2012;5:7531–5.

[26] Moury R, Demirci UB, Ban V, Filinchuk Y, Ichikawa T, Zeng L, Goshome K, Miele P. Lithium hydrazinidoborane: a polymorphic material with potential for chemical Hydrogen storage. Chem Mater 2014;26:3249–55.

[27] Moury R, Demirci U B, Ichikawa T, Filinchuk Y, Chiriac R, van Der Lee A, Miele P. Sodium hydrazinidoborane: a chemical hydrogen-storage material. Chem Sus Chem 2013;6:667–73.

[28] Pylypko S, Petit JF, Ould-Amara S, Hdhili N, Taihei A, Chiriac R, Ichikawa T, et al. Metal hydride-hydrazine borane: towards hydrazinidoboranes or composites as hydrogen carriers. Int J Hydrogen Energy 2015;40:14975-884.

[29] Chua YS, Pei Q, Ju X, Zhou W, Udovic TJ, Wu G, Xiong Z, et al. Alkali metal hydride modification on hydrazine borane for improved dehydrogenation. J Phys Chem C 2014;118:11244–51.

[30] Banu T, Se K, Ash T, Das AK. Dehydrogenation of lithium hydrazinidoborane: insight from computational analysis. Int J Hydrogen Energy 2016;41:18953–62.

[31] Li T, Zhang JG. Theoretical sudy of the metal-controlled dehydrogenation mechanism of $MN_2H_3BH_3$ (M = Li, Na, K): a family of hydrogen storage material. J Phys Chem A 2016;122:1344–9.

[32] Kim DY, Singh NJ, Lee MH, Kim KS. Hydrogen-release mechanisms in lithium amidoboranes. Chem Eur J 2009;15:5598–604.

[33] Shevlin SA, Kerkeni B, Guo ZX. Dehydrogenation mechanisms and thermodynamics of MNH_2BH_3 (M = Li, Na) metal amidoboranes as predicted from first principles. Phys Chem Chem Phys 2011;13:7649–59.

[34] a) Wolstenholme DJ, Titah JT, Che FN, Traboulsee KT, Flogeras J, McGrady GS. Homopolar dihydrogen bonding in alkali-metal amidoboranes and its implications for hydrogen storage. J Am Chem Soc 2011;133:16598–604; b) Wolstenholme DJ, Flogeras J, Che FN, Decken A, McGrady GS. Homopolar dihydrogen bonding in alkali-metal amidoboranes: crystal engineering of low-dimensional molecular materials. J Am Chem Soc 2013;135:2439–42.

[35] Tan Y, Chen X, Chen J, Gu Q, Yu X. The decomposition of α-$LiN_2H_3BH_3$: an unexpected hydrogen release from a homopolar proton-proton pathway. J Mater Chem A 2014;2:15627-32.

[36] a) Kazakov IV, Butlak AV, Shelyganov PA, Suslonov VV, Timoshkin AY. Reversible structural transformations of rubidium and cesium amidoboranes. Polyhedron 2017;127:186–90; b) Owarzany R, Jaroń T, Leszczyński PJ, Fijalkowski KJ, Grochala W. Amidoboranes of rubidium and caesium: the last missing members of the alkali metal amidoborane family. Dalton Trans 2017;46:16315–20.

[37] Weng B, Wu Z, Li Z, Yang H. Hydrogen generation from hydrolysis of MNH_2BH_3 and NH_3BH_3/MH (M = Li, Na) for fuel cells based unmanned submarine vehicles application. Energy 2012;38:205–11.

[38] a) Eaton GR. NMR of boron compounds. J Chem Educ 1969;46:547–56; b) Smith WL. Boron-11 nmr. J Chem Educ 1977;54:469–73; c) Hermanek S. Boron-11 NMR spectra of boranes, main-group heteroboranes, and substituted derivatives. Factors influencing chemical shifts of skeletal atoms. Chem Rev 1992;92:325–62.

[39] Xiong Z, Yong CK, Wu G, Chen P, Shaw W, Karkamkar A, Autrey T, et al. High-capacity hydrogen storage in lithium and sodium amidoboranes. Nature Mater 2008;7:138–41.

[40] Stowe AC, Shaw WJ, Linehan JC, Schmid B, Autrey T. *In situ* solid state ^{11}B MAS-NMR studies of the thermal decomposition of ammonia borane: mechanistic studies of the hydrogen release pathways from a solid state hydrogen storage material. Phys Chem Chem Phys 2007;9:1831–6.

[41] Kobayashi T, Gupta S, Caporini MA, Pecharsky VK, Pruski M. Mechanism of solid-state thermolysis of ammonia borane: a ^{15}N NMR study using fast magic-angle spinning and dynamic nuclear polarization. J Phys Chem. C 2014;118:19548−55.

[42] Kim DY, Lee HM, Seo J, Kim SK, Kim KS. Rules and trends of metal cation driven hydride-transfer mechanisms in metal amidoboranes. Phys Chem Chem Phys 2010;12: 5446−53.

[43] Zhang Y, Autrey T, Wolverton C. First-principles of intermediate products in the decomposition of metal amidoboranes. J Phys Chem C 2012;116:26728−34.

[44] Kim DP, Moon KT, Kho JG, Economy J, Gervais C, Babonneau F. Synthesis and characterization of poly-(aminoborane) as a new boron nitride precursor. Polym Adv Technol 1999;10:702–12.

[45] Gervais C, Maquet J, Babonneau F, Duriez C, Framery E, Vaultier M, Florian P, et al. Chemically derived BN ceramics: extensive ^{11}B and ^{15}N solid-state NMR study of a preceramic polyborazilene. Chem Mater 2001;13:1700–7.

[46] Gervais C, Framery E, Duriez C, Maquet J, Vaultier M, Babonneau F. ^{11}B and ^{15}N solid-state NMR investigation of a boron nitride preceramic polymer prepared by ammonolysis of borazine. J Eur Ceram Soc 2005;25:129–35.

[47] Li L, Gu Q, Tang Z, Chen X, Tan Y, Li Q, Yu X. Two novel derivatives of ammonia borane for hydrogen storage: synthesis, structure, and hydrogen desorption investigation. J Mater Chem A 2013;1:12263–9.

[48] Roy B, Hajari A, Manna J, Sharma P. Supported ammonia borane decomposition through enhanced homopolar B-B coupling. Dalton Trans 2018;47:6570–9.

[49] Luedtke AT, Autrey T. Hydrogen release studies of alkali amidoboranes. Inorg Chem 2010;49:3905–10.

[50] Summerscales OT, Gordon JC. Regeneration of ammonia borane from spent fuel materials. Dalton Trans 2013;42:10075–84.

[51] Kang X, Fang Z, Kong L, Cheng H, Yao X, Lu G, Wang P. Ammonia borane destabilized by lithium hydride: an advanced on-board hydrogen storage material. Adv Mater 2008;20: 2756–9.

[52] Chen J, He T, Wu G, Xiong Z, Chen P. Synthesis and hydrogen storage properties of lithium borohydride amidoborane complex. Int J Hydrogen Energy 2013;38:10944–9.

[53] Moury R, Petit JF, Demirci UB, Ichikawa T, Miele P. Pure hydrogen-generating "doped" sodium hydrazinidoborane. Int J Hydrogen Energy 2015;40:7475–82.

[54] Fijalkowski KJ, Grochala W. Substantial emission of NH_3 during thermal decomposition of sodium amidoborane, $NaNH_2BH_3$. J Mater Chem 2009;19:2043–50.

[55] Shimoda K, Zhang Y, Ichikawa T, Mitaoka H, Kojima Y. Solid state NMR study on the thermal decomposition pathway of sodium borohydride $NaNHBH_3$. J Mater Chem 2011;21:2609–15.

[56] Yuan S, Journet C, Linas S, Garnier V, Steyer P, Benayoun S, Brioude A, et al B. How to increase the h-BN crystallinity of microfilms and self-standing nanosheets: a eeview of the different strategies using the PDCs route. Crystals 2016;6:55.

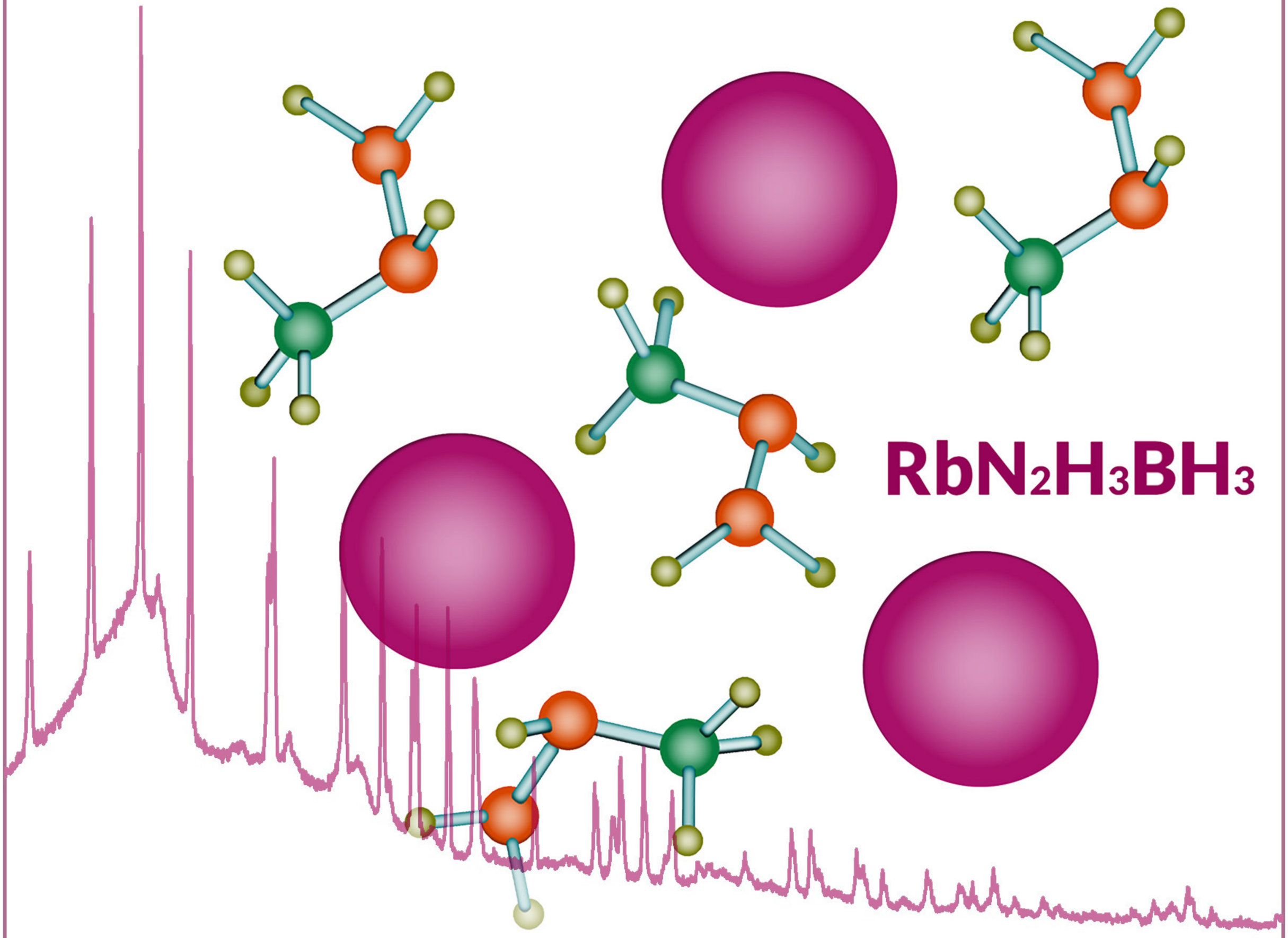
RbN2H3BH3